A&A 466, 839–846 (2007)
DOI: 10.1051/0004-6361:20066683

Astronomy & Astrophysics

The nature of the X-ray flash of August 24 2005

Photometric evidence for an on-axis $z = 0.83$ burst with continuous energy injection and an associated supernova?⋆,⋆⋆

J. Sollerman[1,2], J. P. U. Fynbo[1], J. Gorosabel[3], J. P. Halpern[4], J. Hjorth[1], P. Jakobsson[1,5], N. Mirabal[4], D. Watson[1], D. Xu[1], A. J. Castro-Tirado[3], C. Féron[1], A. O. Jaunsen[6], M. Jelínek[3], B. L. Jensen[1], D. A. Kann[7], J. E. Ovaldsen[6], A. Pozanenko[8], M. Stritzinger[1], C. C. Thöne[1], A. de Ugarte Postigo[3], S. Guziy[3], M. Ibrahimov[9], S. P. Järvinen[10,11], A. Levan[5], V. Rumyantsev[12], and N. Tanvir[5,13]

[1] Dark Cosmology Centre, Niels Bohr Institute, University of Copenhagen, Juliane Maries Vej 30, 2100 Copenhagen Ø, Denmark
[2] Stockholm Observatory, Department of Astronomy, AlbaNova, 106 91 Stockholm, Sweden
[3] Instituto de Astrofísica de Andalucía (IAA-CSIC), PO Box 3.004, 18.080 Granada, Spain
[4] Columbia Astrophysics Laboratory, 550 West 120th Street, Columbia University, New York, NY 10027-6601, USA
[5] Centre for Astrophysics Research, University of Hertfordshire, Collage Lane, Hatfield, Herts, AL10 9AB, UK
[6] Institute of Theoretical Astrophysics, PO Box 1029, 0315 Oslo, Norway
[7] Thüringer Landessternwarte Tautenburg, Sternwarte 5, 07778 Tautenburg, Germany
[8] Space Research Institute (IKI), 84/32 Profsoyuznaya Str, Moscow 117997, Russia
[9] Ulugh Beg Astronomical Institute, Tashkent 700052, Uzbekistan
[10] Astrophysikalisches Institut Potsdam, An der Sternwarte 16, 14482 Potsdam, Germany
[11] Astronomy Division, PO Box 3000, 90014 University of Oulu, Finland
[12] Crimean Laboratory of Sternberg Astronomical Institute MSU, Nauchny, Crimea, 98409, Ukraine
[13] Department of Physics and Astronomy, University of Leicester, Leicester, LE1 7RH, UK

Received 2 November 2006 / Accepted 18 January 2007

ABSTRACT

Aims. Our aim is to investigate the nature of the X-Ray Flash (XRF) of August 24, 2005.
Methods. We present comprehensive photometric *R*-band observations of the fading optical afterglow of XRF 050824, from 11 min to 104 days after the burst. In addition we present observations taken during the first day in the *BRIK* bands and two epochs of spectroscopy. We also analyse available X-ray data.
Results. The *R*-band lightcurve of the afterglow resembles the lightcurves of long duration Gamma-Ray Bursts (GRBs), i.e., a power-law, albeit with a rather shallow slope of $\alpha = 0.6$ ($F_\nu \propto t^{-\alpha}$). Our late *R*-band images reveal the host galaxy. The rest-frame *B*-band luminosity is $\sim 0.5\ L^*$. The star-formation rate as determined from the [O II] emission line is $\sim 1.8\ M_\odot\ \mathrm{yr}^{-1}$. When accounting for the host contribution, the slope is $\alpha = 0.65 \pm 0.01$ and a break in the lightcurve is suggested. A potential lightcurve bump at 2 weeks can be interpreted as a supernova only if this is a supernova with a fast rise and a fast decay. However, the overall fit still shows excess scatter in the lightcurve in the form of wiggles and bumps. The flat lightcurves in the optical and X-rays could be explained by a continuous energy injection scenario, with an on-axis viewing angle and a wide jet opening angle ($\theta_j \gtrsim 10°$). If the energy injections are episodic this could potentially help explain the bumps and wiggles.
Spectroscopy of the afterglow gives a redshift of $z = 0.828 \pm 0.005$ from both absorption and emission lines. The spectral energy distribution (SED) of the afterglow has a power-law ($F_\nu \propto \nu^{-\beta}$) shape with slope $\beta = 0.56 \pm 0.04$. This can be compared to the X-ray spectral index which is $\beta_X = 1.0 \pm 0.1$. The curvature of the SED constrains the dust reddening towards the burst to $A_v < 0.5$ mag.

Key words. cosmology: observations – gamma rays: bursts

1. Introduction

X-Ray Flashes (XRFs) are similar to Gamma-Ray Bursts (GRBs), but with most of the fluence of the prompt emission detected in the X-ray band. Their existence as a class was suggested by Heise et al. (2001) based on data from the BeppoSAX satellite.

The high energy spectra (νF_ν) of the prompt emission from GRBs are well described by the so-called Band function (Band et al. 1993), which is composed of two smoothly connected power-laws. The energy at which the two power-laws connect, $E_{\rm peak}$, is where most of the energy is emitted. For classical GRBs, $E_{\rm peak}$ is typically a few 100 keV (Preece et al. 2000). The spectra of the prompt emission of XRFs are also well fitted by the Band function, but with values of $E_{\rm peak}$ below $\lesssim$50 keV and in some cases even below 10 keV (Kippen et al. 2003; Barraud et al. 2003).

⋆ This paper is based on observations from a multitude of telescopes, for example on observations made with ESO Telescopes at the Paranal Observatory (programme ID 075.D-0270) and with the NTT and ESO/Danish 1.5-m telescope at the La Silla Observatory. Also based on observations made with the Nordic Optical Telescope, operated on the island of La Palma jointly by Denmark, Finland, Iceland, Norway, and Sweden, in the Spanish Observatorio del Roque de los Muchachos of the Instituto de Astrofisica de Canarias.
⋆⋆ Table 2 is only available in electronic form at `http://www.aanda.org`

Sakamoto et al. (2005) argue, in accordance with previous studies, that the spectral distributions of XRFs, X-ray Rich GRBs and GRBs form a continuum, suggesting that they all arise from the same phenomenon (see also Barraud et al. 2003, 2005). There has also been growing evidence that (at least some) XRFs are the result of classical GRBs seen off-axis (Yamazaki et al. 2002, 2003; Rhoads 2003; Fynbo et al. 2004; Granot et al. 2005).

Other suggestions include XRFs as either dirty fireballs, which are relativistic jets with a larger baryon load and hence (assuming external shocks) lower Γ-factors than those of classical GRBs (Dermer et al. 1999; Heise et al. 2001), or XRFs as clean fireballs where (assuming internal shocks) the spread in Γ-factors is small but the average Γ-factor is large (Barraud et al. 2005).

However, there are still open questions regarding the origin of XRFs. While the connection between long GRBs and certain core-collapse supernovae appears to be well established (Hjorth et al. 2003; Matheson et al. 2003; Zeh et al. 2004), the case has not been as well defined for XRFs. Fynbo et al. (2004) performed the first comprehensive observational campaign of an XRF optical afterglow, for XRF 030723 (see also Butler et al. 2005). The well sampled lightcurve for XRF 030723 displayed several interesting features:

(i) The very early lightcurve was essentially flat, in accordance with models for which XRFs are viewed away from the jet axis.
(ii) The following power-law decay was very similar to that seen in typical GRBs, suggesting a common origin.
(iii) At ∼16 days past burst a strong bump in the lightcurve suggested the presence of a fast rising supernova. The supernova interpretation was argued to be consistent with the spectral energy distribution (SED) evolution (Fynbo et al. 2004) and was later supported by modeling both of the afterglow (Granot et al. 2005) and of the supernova (Tominaga et al. 2004).

More evidence has now been presented arguing for a common origin for GRBs and XRFs. XRF 020903 had a late lightcurve and spectrum consistent with a supernova at $z = 0.25$ (Soderberg et al. 2005; Bersier et al. 2006). More recently, the nearby ($z = 0.0331$, Mirabal & Halpern 2006; Wiersema et al. 2007) and unusual burst, XRF 060218, with a very low $E_{\rm peak} \sim 5$ keV (Campana et al. 2006) showed unambiguous evidence for an associated supernova (e.g., Sollerman et al. 2006; Modjaz et al. 2006; Mirabal et al. 2006; Pian et al. 2006). SN 2006aj associated with XRF 060218 clearly established the close link between SNe, (GRBs) and XRFs.

However, other XRFs with late time coverage did apparently not show any clear evidence for a supernova bump (Soderberg et al. 2005; Levan et al. 2005). This could point to a difference in the origin of XRFs and the long GRBs with accompanying SNe (but see the recent paper by Fynbo et al. 2006, for GRBs with no associated supernova emission), although any such claim has to await observations of XRFs with a better determined distance scale. Most of the XRFs claimed to lack SNe in the above-mentioned studies had no measured redshifts.

We here present data for XRF 050824 for which we have obtained a well monitored optical lightcurve and a secure spectroscopic redshift.

1.1. XRF 050824

XRF 050824 was detected by the BAT instrument on-board the Swift satellite (Campana et al. 2005a) on August 24.9669 2005 UT (Universal Time is used throughout the article). The burst duration (T_{90}) was 25 s, i.e., this was a long-duration burst. The total fluence in the 15–150 keV band was $\sim 2.3 \times 10^{-7}$ erg cm^{-2} (Krimm et al. 2005). The burst was also detected by the FREGATE instrument onboard HETE-2 (Crew et al. 2005). As seen by HETE-2 the value of the fluence ratio $S(2-30)/S(30-400) = 2.7$. Crew et al. (2005) estimated $E_{\rm peak} < 12.7$ keV. GRB 050824 is thus clearly an XRF.

The BAT on-board localization was reported to an accuracy of 3 arcmin. Early ROTSE-III data did not detect any new object (Schaefer et al. 2005), but our observations starting 38 min after the trigger revealed a new object at RA = 00:48:56.1, Dec = +22:36:32 (J2000, see Sect. 3.1), which we later confirmed as the counterpart (Gorosabel et al. 2005).

In this paper we focus on our comprehensive optical study of this afterglow. The article is organized as follows. Section 2 outlines how the optical observations were obtained and reduced. The results are presented in Sect. 3, which includes the astrometry, the optical lightcurve, the spectral energy distribution, the spectroscopic results, data on the host galaxy and an analysis of available X-ray data of the afterglow. Finally, we end the paper with a discussion (Sect. 4) and some conclusions (Sect. 5).

Table 1. Telescopes and Instruments.

Telescope	Instrument/ CCD	FOV (arcminutes)	Pixel scale (arcsec pixel^{-1})
BOOTES-1B	ST8E	40×26	1.6
OSN	ROPER	7.92×7.92	0.232
NOT	ALFOSC	6.3×6.3	0.189
NOT	STANCAM	3×3	0.176
D1.5 m	DFOSC	13.7×13.7	0.395
MDM 1.3 m	SITe CCD	8.6×8.6	0.508
MDM 2.4 m	SITe CCD	9.4×9.4	0.275
CrAO2.6	FLI-IMG1001E	8.5×8.5	0.5
Maidanak1.5 m	SITe CCD	8.5×3.5	0.266
WHT	ULTRACAM	5×5	0.3
NTT	EMMI	9.9×9.1	0.33
VLT	FORS1	6.8×6.8	0.20
VLT	FORS2	6.8×6.8	0.25
VLT	ISAAC	2.5×2.5	0.148

2. Observations

2.1. Photometry

Our very first observations of XRF 050824 were obtained with the BOOTES-1B 30 cm robotic telescope (e.g., Castro-Tirado et al. 2004) in southern Spain, which detected the burst from 10.6 min after the high energy event in several R-band exposures. However, since these images were not processed until later, the actual discovery was instead made via the studies we initiated 38 min after the burst (Gorosabel et al. 2005) using the 1.5 m telescope at the Observatorio de Sierra Nevada (OSN).

We conducted a comprehensive study of the optical afterglow over the following 100 days using several telescopes and instruments. In Table 1 we summarize the telescopes and instruments used and provide details on the field-of-view (FOV) and pixel scale of these instruments.

We used the ESO/Danish 1.54 m telescope (D1.5m) on La Silla equipped with the DFOSC instrument, the 2.56 m Nordic Optical Telescope (NOT) on La Palma equipped with ALFOSC and STANCAM. We also used the 1.3 m MDM telescope (in August 2005) and the 2.4 m MDM telescope

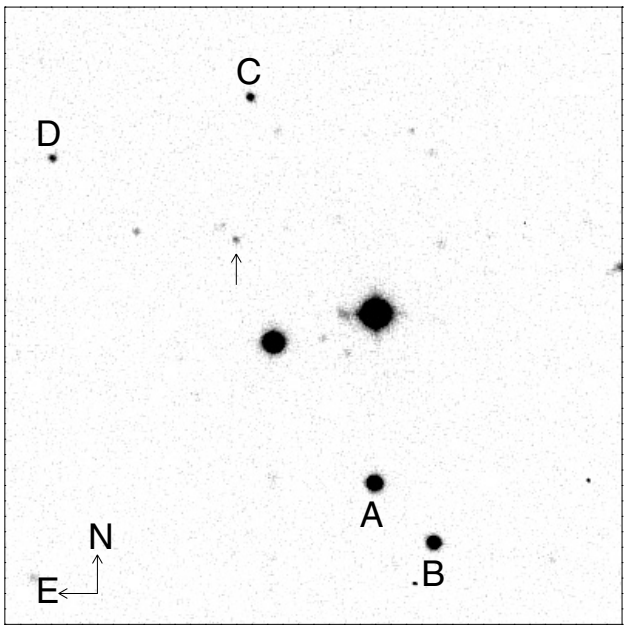

Fig. 1. The 156 × 156 arcsec^2 field around the position of XRF 050824 in a D1.5m *R*-band image taken 6 h after the burst. East is to the left and North is up. The position of the afterglow is marked with an arrow and the four local calibration stars are marked with capital letters.

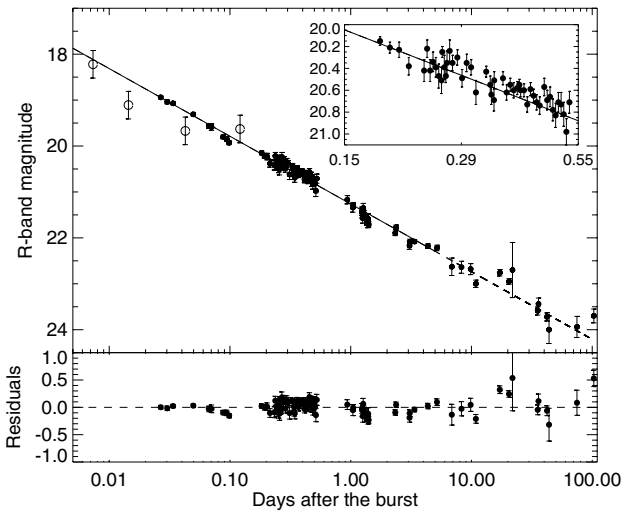

Fig. 2. The *R*-band lightcurve of the afterglow of XRF 050824. The line represents a power-law decay with decay slope $\alpha = 0.59$. The open circles represent the BOOTES detections. The inset highlights the well sampled phase at 0.15–0.55 days, and the lower panel shows the residuals from the best power-law fit.

Table 3. Local calibration stars.

ID	*B*	*V*	*R*	*I*
Star A	17.42	16.60	16.18	15.60
Star B	18.17	17.29	16.83	16.18
Star C	–	20.23	19.14	17.75
Star D	–	20.66	19.54	17.77

(in September), the Crimean Astrophysical Observatory (CrAO) 2.6 m telescope and the 1.5 m telescope at the Maidanak observatory.

Late observations were also obtained at the ESO New Technology Telescope (NTT) at La Silla and at the Very Large Telescope (VLT) on Paranal, Chile. A single epoch near infrared (near-IR) *K*s image was obtained using the VLT/ISAAC instrument.

The full journal of observations is given in Table 2. The data were reduced using standard techniques for de-biasing and flat-fielding.

2.2. Spectroscopy

Spectra of the source were obtained with the VLT at two epochs. A 2 × 1500 s spectrum was obtained on August 25.4, about 0.4 days past the burst, when the afterglow had a magnitude of $R \approx 20.7$. We used the FORS2 spectrograph with a 300V grism, the GG375 order separation filter and a 1.0 arcsec wide slit providing a dispersion of 13.3 Å over the spectral region from 3800 Å to 8900 Å.

The following night, on August 26.3, when the afterglow had faded by one magnitude, we obtained another spectrum of 6 × 1500 s exposure time. The instrumental setup was identical to that used on the first night.

We extracted the spectrum using standard procedures within `IRAF`. Wavelength calibration was obtained using images of HeNeAr lamps obtained as part of the morning calibrations. Flux calibration was performed using spectra of the spectrophotometric standard star G138-31 (Oke 1990).

3. Results

3.1. Astrometry

We determined the celestial position of the XRF 050824 optical afterglow as the mean astrometric solution found in 10 OSN *R*-band images. Each afterglow position is based on ~50 USNO-A2.0 reference stars per image. The mean value of the coordinates are:

RA(J2000) = 00:48:56.14 ± 0.03s,
Dec (J2000) = +22:36:33.2 ± 0.4″.
These astrometric errors include the 0.25″ systematic error of the USNO-A2.0 catalogue (Assafin et al. 2001; Deutsch 1999).

3.2. The lightcurve

The photometry of the XRF was carried out using either PSF fitting photometry (when the afterglow was bright) or aperture photometry (at later times when the host started to contribute significantly). We measured the magnitudes of the optical afterglow as well as 4 stars in the field. The relative magnitudes were transformed to the standard system using observations of photometric standard stars (Landolt 1992). The local standard stars are marked in Fig. 1, and their magnitudes are given in Table 3. The zeropoint uncertainties are of the order of 0.03 mag.

In Fig. 2 we have plotted the *R*-band lightcurve ranging from 11 minutes to 104 days after the XRF. This includes the early detections from the BOOTES telescope (open circles). The best fit power-law has a slope of $\alpha_R = 0.59 \pm 0.01$ ($F_\nu \propto t^{-\alpha}$) and is also indicated in the figure.

The *I*-band lightcurve follows the *R*-band very well during the first day when we have observations in both bands. The slope is consistent with the *R*-band lightcurve ($\alpha_I = 0.51 \pm 0.06$, whereas $\alpha_R = 0.57 \pm 0.03$ for the same period).

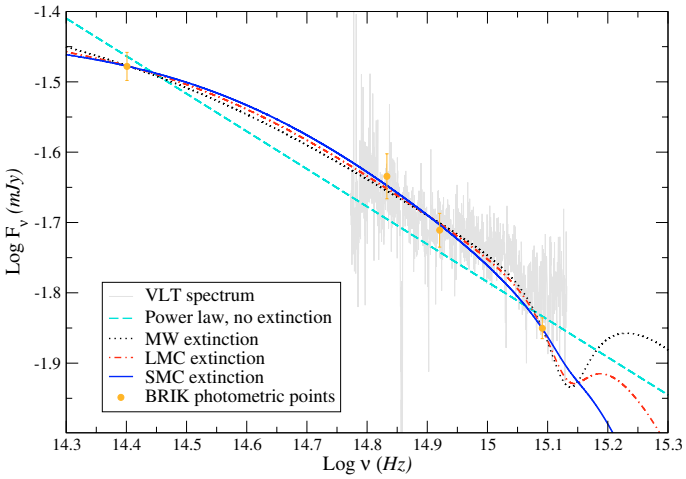

Fig. 3. The spectral energy distribution for XRF 050824. These are the *AB* magnitudes in *B*, *R*, *I*, and *K* corrected for Galactic extinction of $E(B-V) = 0.035$ mag with $R_V = 3.1$, and interpolated to the same epoch at ∼0.4 days past explosion.

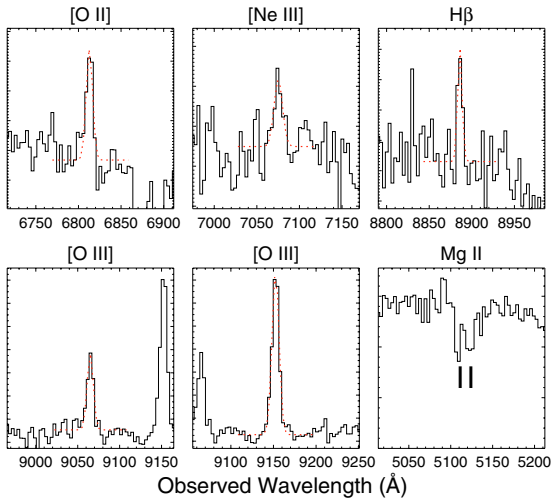

Fig. 4. Emission lines from the VLT spectra and overplotted Gaussian fits. We refer to Table 4 for the measurements. Lower right panel shows the Mg II absorption lines. The tickmarks indicate the expected positions for this doublet line given the redshift determined from the emission lines.

3.3. Spectral energy distribution

The multiband observations of XRF 050824 allowed us to construct the spectral energy distribution (SED) of the burst at an epoch of ∼0.4 days.

The result is presented in Fig. 3 where we have converted the *B*, *R*, *I* and *K* band magnitudes into *AB* magnitudes. The optical and near-IR magnitudes were corrected for Galactic reddening of $E(B-V) = 0.035$ mag (Schlegel et al. 1998) and transformed to flux densities using the conversion factors given by Fukugita et al. (1995) and Allen (2000), respectively. Given that the multiband observations were not all performed at the same epoch, their corresponding fluxes were rescaled using the best fit power law.

A power-law fit in the form $F_\nu \propto \nu^{-\beta}$ provides a tolerable fit for the SED. The spectral index is $\beta = 0.56 \pm 0.04$, assuming negligible extinction.

Unfortunately, with the available data we cannot say much about the extinction. The SMC, LMC or Milky Way extinction laws give equally good fits to the data (Fig. 3). Fixing the redshift at $z = 0.83$ (see Sect. 3.4), a free fit with an intrinsic power-law shape of the SED and an SMC like extinction curve from Pei (1992) implies an extinction of $A_V = 0.4 \pm 0.2$ mag. However, this would give an unrealistically flat $\beta \sim 0$ spectrum. Given the sparse dataset the only thing we can firmly conclude is that A_V is less than 0.5 mag. A low value of the global extinction is also implied by the blue color of the host galaxy (Sect. 3.5).

3.4. The spectra

The combined flux-calibrated spectrum is also included in Fig. 3. The slope is consistent with the contemporary photometry.

We determined the redshift from the first night's spectrum (Fynbo et al. 2005) using emission lines such as [O II] λ3727, [O III] $\lambda\lambda$4959, 5007 and Hβ. As noted by Fynbo et al. (2005), we also detect absorption lines from Mg II at this redshift. We discuss this further below (Sect. 4.1). The lines are shown in Fig. 4 and the measured positions and fluxes of the lines are given in Table 4. The redshift is $z = 0.828 \pm 0.005$. Note that the fluxes given in Table 4 are not corrected for Galactic or host galaxy extinction. The uncertainties in absolute line fluxes can be up to 30%.

Using a cosmology where $H_0 = 70$ km s^{-1} Mpc^{-1}, $\Omega_\Lambda = 0.7$ and $\Omega_m = 0.3$, this redshift corresponds to a luminosity distance of 5.24 Gpc. This distance will be used hereafter.

3.5. The host galaxy

Our late *R*-band image from December 7, 2005, 104 days past explosion, shows an extended source with magnitude $R = 23.70 \pm 0.15$ at the position of the afterglow. This is the host galaxy of XRF 050824. An image obtained under very good seeing conditions at VLT in October 2005 is shown in Fig. 5. Note that all late observations (past 35 days) are consistent with this being the host, with little contribution from the afterglow (or a supernova).

The host magnitude is 23.6 when corrected for a Galactic extinction of $E(B-V) = 0.035$ mag. At the redshift of this galaxy the *R* band corresponds to the rest frame *U* band. However, comparison of the absolute luminosity with other galaxies is often made in the rest frame *B* band. To do so we need to make some assumption about the color of the host. Here we note that the *BVR* magnitudes from our latest VLT data, when the host is clearly dominating the emission, are very similar to the magnitudes of the host of GRB 000210 (Gorosabel et al. 2003) at a similar redshift.

We therefore conclude that the absolute luminosity of the XRF 050824 host is very similar to the one determined by Gorosabel et al. (2003), i.e., $L = 0.5 \pm 0.2\ L_\star$ in the rest frame *B* band.

The host is extended with a size of roughly 0.8 arcsec, which at a distance of 5.24 Gpc corresponds to a linear scale of ∼6 kpc. Finally, from the [O II] lines we can estimate the star formation rate (SFR). The flux of this line, corrected for Galactic extinction, corresponds to a SFR of 1.8 $M_\odot$ yr^{-1}, following Kennicutt (1998).

In fact, using the extinction corrected value for the flux of Hβ, and assuming a case B recombination ratio for Hα versus Hβ, we can also use this line to estimate that the SFR is 1.8 $M_\odot$ yr^{-1}, again following Kennicutt (1998). As usual, any slit-losses would increase this number. We note that the

Table 4. Spectral line measurements.

ID	Rest wavelength (Å)	Observed wavelength (Å)	Flux (10^{-17} erg s^{-1} cm^{-2})	Redshift
[O II]	3727.42	6812.94	3.5	0.828
[Ne III]	3868.75	7075.00	2.0	0.828
Hβ	4861.33	8885.96	2.4	0.828
[O III]	4958.91	9064.99	6.0	0.828
[O III]	5006.84	9152.43	14.7	0.828
Mg II	2800.0	5117.63	–	–

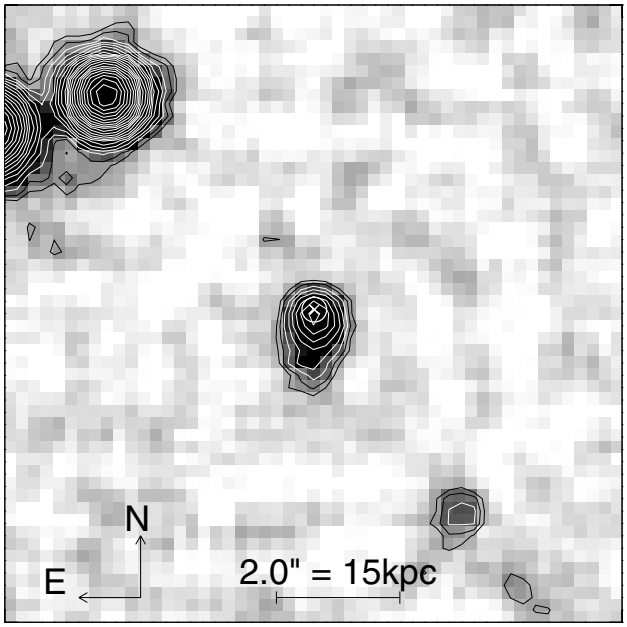

Fig. 5. The 10 × 10 arcsec^2 field around the position of XRF 050824 from our latest VLT *R*-band image 42 days after the burst. East is to the left and North is up. The position of the afterglow is marked with a cross and the 3-sigma error circle on the position of the afterglow. The host has a magnitude of $R = 23.7$. The *FWHM* of pointlike objects is 0.5 arcsec in this image.

consistency of the Hα and [O II] predictions of the SFR also supports the notion of low extinction in the host galaxy.

This SFR compares rather well with the estimate for the host of GRB 000210 mentioned above, which has similar properties and an estimated SFR from the UV light of $2.1 \pm 0.2\ M_\odot\ \mathrm{yr}^{-1}$ (Gorosabel et al. 2003).

The specific star formation rate for the host galaxy of XRF 050824 is thus only $\sim 4\ M_\odot\ \mathrm{yr}^{-1}(L/L^\star)^{-1}$. This is rather low, but not exceptional, and falls well within the population of small star-forming blue galaxies as shown in Fig. 2 of Sollerman et al. (2005), (see also Christensen et al. 2004).

Finally, we can estimate the metallicity of the galaxy using the R23 technique (Pagel 1979). Using the results presented in Table 4 and applying $E(B-V) = 0.035$ mag, we derive $\log(R_{23}) = 1.0$. This is quite high, and indicates a metallicity (just) below solar (see e.g., Fig. 5 by Kewley & Dopita 2002). However, the small number of emission lines in the analysis makes this estimate rather uncertain.

The star formation rate and size thus indicates a fairly normal galaxy, similar to other GRB host galaxies (e.g., Le Floc'h et al. 2003; Christensen et al. 2004; Sollerman et al. 2005). The metallicity confirms the trend that GRB host galaxies have sub-solar metallicities. The luminosity is not particularly low compared to other GRB hosts, but is similar to the host of XRF 050416A (Soderberg et al. 2006).

3.6. The X-rays

Swift-XRT did not observe the burst immediately due to a lunar constraint and the XRT began observations about 6000 s after the burst trigger (Campana et al. 2005b). We have analysed the standard processed XRT data starting at 0.4 days after the burst using version 2.3 of the Swift software. Background-subtracted spectra and lightcurves were extracted in a standard way with circular source and background extraction apertures of 30″ and 60″ radius for the PC-mode data. Data from the WT-mode were not used because they added very little signal.

The combined spectrum was fit with a single absorbed power-law with absorption at the Galactic level ($N_\mathrm{H} = 3.62 \times 10^{20}$ cm^{-2}, Dickey & Lockman 1990) and gave an acceptable fit ($\chi^2 = 43.7$ for 40 degrees of freedom). Adding an absorber at the redshift of the host galaxy gives a better fit ($\chi^2 = 30.4$ for 39 degrees of freedom) with an equivalent hydrogen column density of $N_\mathrm{H} = 1.8^{+0.7}_{-0.6} \times 10^{21}$ cm^{-2} and a power-law photon index $\beta_\mathrm{X} = 1.0 \pm 0.1$. The absorption model has abundance ratios fixed at solar values. The soft X-ray absorption is dominated by α-chain elements and is therefore a measure of the metal absorption and is regardless of whether the elements are in the gas or solid phase (see Watson et al. 2006; Turnshek et al. 2003).

The flux decay of the afterglow followed a single power-law with decay index, $\alpha_\mathrm{X} = 0.75 \pm 0.04$, with the fit being marginally acceptable ($\chi^2 = 24.8$ for 16 degrees of freedom, null hypothesis probability = 0.07). This decay rate is somewhat faster than the average slope seen in the optical lightcurve (albeit there could be a break in the optical light curve, see Sect. 4.2.2). Note, however, that the X-ray data are not very constraining at the later phases.

4. Discussion

4.1. Absorption line redshift

As noted in Sect. 3.4 the spectra also include absorption lines from Mg II. These lines are seen at both epochs, but are most clearly detected in the first epoch, which has the best signal-to-noise ratio. The lines are displayed in Fig. 4, and the redshift is consistent with the estimate from the emission lines.

That the redshift can be determined from both emission lines and absorption lines is of some importance. The distance scale of the XRFs has only recently been shown to be cosmological. The first spectroscopic redshift of $z = 0.25$ for XRF 020903 (Soderberg et al. 2005) was based on emission lines only. In principle, a single case could be affected by a superposed and unrelated galaxy, but now XRF 050416A also has a measured emission line redshift ($z = 0.65$, Cenko et al. 2005; Soderberg et al. 2006) as has GRB/XRF 030528 ($z = 0.78$, Rau et al. 2005).

The GRB 030429 studied by Jakobsson et al. (2004) also displayed absorption lines. It showed an $E_{\rm peak}$ of 35 keV at a redshift of $z = 2.66$, and is thus a borderline case, consistent with an X-ray Rich burst. More recently, the rather unusual XRF 060218 had a secure redshift from both emission lines and absorption lines ($z = 0.033$, Mirabal & Halpern 2006; Wiersema et al. 2007; Pian et al. 2006).

These findings, together with the robust redshift determination for the rather normal XRF 050824, have therefore proven the cosmological distance scale for these objects beyond doubt.

4.2. The lightcurve of the afterglow

Our R-band lightcurve of XRF 050824 is one of the best sampled optical lightcurves for an XRF. The most conspicuous aspect of this lightcurve is that it is basically consistent with a power-law for the entire duration (Fig. 2). The best fit power law $\alpha = 0.6$ is quite a slow decay.

4.2.1. The early times

One of the more interesting aspects of the lightcurve is that it declines steadily from very early on. This is in stark contrast to the lightcurve of XRF 030723 (Fig. 6), which apparently had a constant lightcurve for the first day after the burst.

The flat early part of the lightcurve of XRF 030723 was interpreted in terms of geometry (Fynbo et al. 2004), where an off-axis orientation can make an increasingly large fraction of the jet visible and thus maintain a constant (or even brightening) lightcurve (Granot et al. 2005). We see no evidence for this in XRF 050824. It's early lightcurve is consistent with the same decay seen throughout the lightcurve. This can thus be seen as evidence for an on-axis burst, which would mean that a geometrical interpretation does not explain the difference between XRFs and GRBs in all cases (see also Soderberg et al. 2006).

4.2.2. A break and a bump in the lightcurve

At first glance the R-band lightcurve shown in Fig. 2 appears consistent with a single power-law decline throughout the entire afterglow. However, since the final points are due to the host galaxy, the data do suggest a break in the lightcurve. As mentioned in Sect. 3.5 the host is extended, so most of the light at these epochs is indeed from the galaxy. This means that the single power law must be broken at an early time, or the later points would have been much brighter. The break in the lightcurve also means that an extra component is needed to explain the excess light at 10−20 days past the burst.

We embarked on simultaneously fitting two power-laws and a stretchable SN 1998bw template, in accordance with the method outlined by Zeh et al. (2004). Fixing the host galaxy magnitude, we were able to constrain a shallow break (from $\alpha = 0.6$ to 0.8) in the lightcurve to occur at ∼0.5 days past burst (Fig. 6). This could be a cooling break. The required supernova is rather unusual. In the notation of Zeh et al. (2004) this is a supernova with $k = 1.05 \pm 0.42$ and $s = 0.52 \pm 0.14$. This is a bright and fast lightcurve and is different from the lightcurve of the canonical SN 1998bw, which is often associated with long GRBs, but is similar to, although brighter than, the supernova associated with XRF 060218. In Fig. 6 we also note the flatter early lightcurve for XRF 030723, the steeper late decay and the conspicuous supernova bump at 20 days past burst.

The actual peak luminosity of the potential supernova associated with XRF 050824 is, however, highly uncertain. If there is internal extinction in the host galaxy the corresponding supernova would have to be brighter, but our SED analysis shows that this can not be a very large effect. This is also supported by the rather blue color of the host galaxy, and by the deduced balmer line ratios. A larger uncertainty arises from the assumptions on the contribution from the afterglow. With SN 1998bw ejecting ∼0.5 $M_\odot$ of ^{56}Ni (e.g., Woosley et al. 1999; Sollerman et al. 2000), we can estimate that a supernova associated with XRF 050824 would have had to eject at least on the order of 0.6 ± 0.3 $M_\odot$ of ^{56}Ni. This is assuming that the peak brightness scales with nickel-mass.

4.2.3. Wiggles, bumps, humps and jitter

In fact, the fit to the lightcurve is not very satisfactory even after invoking a break and a hypothetical supernova bump. This is seen in Fig. 6, where the reduced χ^2 is 1.8. The entire lightcurve of XRF 050824 displays wiggles and humps throughout the time of the observations. The largest deviations are from a systematic dip in the NOT data relative to the overall fit just before 0.1 days, and an increase in the scatter from 2–5 days. These deviations cannot be satisfactorily fitted by a broken power-law scheme that is supposed to model a simple impulsive shock or jet.

Another example is at 0.2–0.5 days past the burst when we have a well monitored lightcurve, in particular from the MDM. This is shown in the inset in Fig. 2. A linear decay is not a formally good fit to these data. There appear to be wiggles around the steady linear decline. Since most of these observations were obtained at the same telescope, and have been reduced in the same way against the same local standards, we do not believe this is purely an instrumental effect. Although the statistical significance is rather low in our lightcurve, we note that similar jittering has been observed previously in GRBs, both in long GRBs (e.g., Gorosabel et al. 2006; Matheson et al. 2003) and in short GRBs (Hjorth et al. 2007), and can be interpreted in terms of variations in the surrounding circumburst medium or as due to prolonged activity of the central engine. Similar explanations can thus be put forward also for this XRF.

4.2.4. Continuous energy injection

Prolonged central engine activity with multiple energy injections could thus be the explanation for the deviations from a perfect power-law (Björnsson et al. 2004). Prolonged activity in terms of continuous energy injection could also explain the slow decline rates in both optical ($\alpha_{\rm R} = 0.65$ when corrected for host galaxy contribution) and in X-rays ($\alpha_{\rm X} = 0.75$). In Fig. 7 we show an example of a model for the afterglow emission in the X-ray and the R band for continuous energy injection. This model is detailed below.

We have modeled the afterglow in terms of a long-term continual energy injection in the forward shock. We consider an uniform relativistic jet undergoing the energy injection from the central source and sweeping up its surrounding uniform medium. The dynamical evolution of the outflow is calculated using the formulae in Huang et al. (2000) and adding an energy injection process with the form $\mathrm{d}E_{\rm inj}/\mathrm{d}t = A(t/t_0)^{-q}$ for $t_0 < t < t_{\rm end}$. The fractions of shock energy given to the electrons $\epsilon_{\rm e}$ and to the magnetic field ϵ_B are assumed to be constant.

The model fits shown in Fig. 7 have the following jet parameters: the isotropic kinetic energy $E_k = 10^{52}$ erg, $\epsilon_{\rm e} = 0.4$,

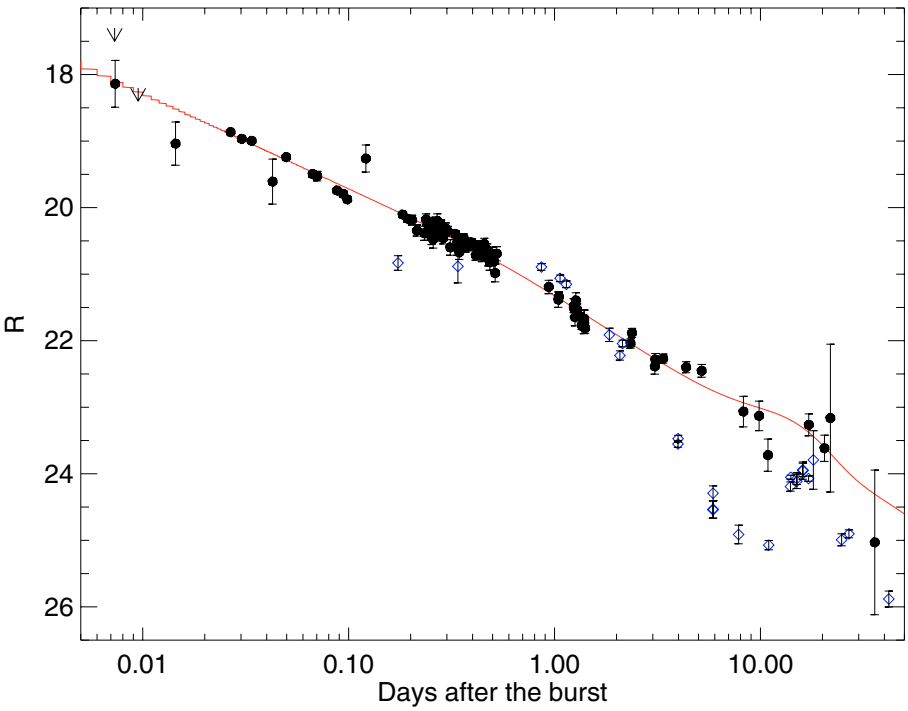

Fig. 6. The *R*-band magnitudes for XRF 050824 corrected for Galactic extinction and for the contribution from the host galaxy (black, filled dots). The (red) line is our fit to these data, following Zeh et al. (2004). The (blue) open diamonds are the observations of XRF 030723 (Fynbo et al. 2004). These are just as observed, i.e., no assumption has been made about the redshift of that burst, although we have corrected for Galactic extinction of $E(B-V) = 0.03$ mag.

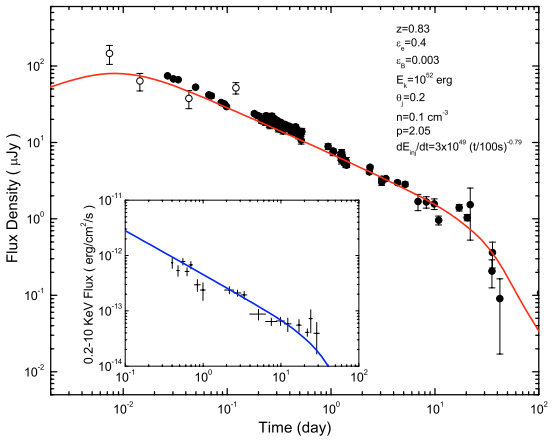

Fig. 7. Modeling *R*-band (host subtracted) and X-ray (inset) afterglow lightcurves of XRF 050824 with continuous energy injection. The fitting parameters are given in the figure and are further discussed in the text.

$\epsilon_B = 0.003$, the circumburst density $n = 0.1$ cm^{-3}, the electron index $p = 2.05$, the half-opening angle $\theta_j = 0.2$, and the viewing angle $\theta_{\rm obs} = 0$ (i.e., on-beam viewing), together with the energy injection parameters: $A = 3 \times 10^{49}$ erg/s, $q = 0.8$, $t_0 = 100$ s, and $t_{\rm end} = 2 \times 10^6$ s. This rather large amount of ejected energy is needed to explain the long and shallow decline; the amount is similar to that found for GRB 050315 (Zhang et al. 2006). Since there is no proper jet break until possibly after a week, the constraint on the jet opening angle of $\theta_{\rm j} \gtrsim 10^\circ$ is quite robust. We did not attempt to fit the very early lightcurve. At these phases it is likely that a reverse shock component is required.

We note again the late re-brightening. At such a late time, the ejecta is only moderately relativistic. The patchy jet model may be unable to account for these variabilities (Kumar & Piran 2000), which may instead be attributed to the re-activity of the central engine (e.g., Fan et al. 2005), or, as mentioned above, to a supernova (Sect. 4.2.2).

4.3. Amati relation

Several XRFs have been shown to follow the same relation as GRBs, that $E_{\rm peak} \propto E_{\rm iso}^{1/2}$ (Amati et al. 2002), where $E_{\rm iso}$ is the isotropic-equivalent radiated energy. For XRF 050824, we can not determine a precise total energy due to the lack of knowledge concerning the peak energy of the BAT spectrum. However, we can calculate lower and upper limits by integrating the best fit power law spectral energy distributions in the $(15-150) \times (1+z)$ keV band and in the the full $1-10^4$ keV band. We obtained 4.1×10^{50} erg $< E_{\rm iso} < 3.4 \times 10^{51}$ erg, which when using the Amati relation, would provide a constraint on the observed peak energy 11 keV $< E_{\rm peak}^{\rm obs} < 32$ keV. This is thus only just in agreement with that from the spectral fitting, $E_{\rm peak}^{\rm obs} < 13$ keV.

Besides this event, the Amati relation is also applicable to XRFs 020903 and possibly 030723 (Lamb et al. 2005), XRF 050416A (Sakamoto et al. 2005) and XRF 050406 (Schady et al. 2006). (See also Amati et al. 2007; Ghisellini et al. 2006, for XRF 060218.)

That this relation holds for both XRFs and classical GRBs not only implies that both classes of bursts can be on-axis events (Amati et al. 2007) but also supports the idea that both can be interpreted under a unified physical mechanism.

5. Conclusions

We have seen that the afterglows of XRFs can appear quite different. The early flat optical lightcurve of XRF 030723 was consistent with predictions of an off-axis burst (Fynbo et al. 2004; Granot et al. 2005). On the contrary, XRF 050824 displays an optical lightcurve which is decaying at a fairly constant, but slow, rate from 10 min after the burst. Our afterglow model indicates this to be an on-axis burst. We have also found some evidence for a bump in the lightcurve, which is consistent with a supernova as fast as that associated with XRF 060218, i.e., considerably faster than the SN 1998bw lightcurve.

Most well observed XRFs with a redshift where a supernova could be expected to emerge do show some evidence for this.

This is similar to the case for ordinary long GRBs (Zeh et al. 2004). A common origin for XRFs and GRBs is therefore likely but there also seems to be several parameters affecting the observables of the burst. In the context of the four-field diagram presented by Sollerman et al. (2006), XRF 050824 should be in the same category as XRF 020903 and XRF 030723; XRFs with an associated supernova but where the optical light is dominated by the afterglow at early phases.

The mounting evidence for supernovae in GRBs and XRFs also shows that there is a large variety in supernova properties (Woosley & Bloom 2006). The emergence of supernovae much fainter (Pian et al. 2006; Sollerman et al. 2006) and much faster (this work) than the canonical SN 1998bw put constraints on the underlying explosion model. Recently, Fynbo et al. (2006) also reported two GRBs where no supernova emission is seen, down to 100 times fainter than SN 1998bw. It is still not clear whether we see two (or more) fundamentally different explosion mechanisms, or if there is a very wide continuum of properties for these blasts.

Acknowledgements. This paper is based on observations collected by the Gamma-Ray Burst Collaboration at ESO (GRACE) at the European Southern Observatory, Paranal and La Silla, Chile. We thank the ESO staff for their help in securing the service mode data reported here. We acknowledge benefits from collaboration within the EU FP5 Research Training Network "Gamma-Ray Bursts: An Enigma and a Tool". This work was also made at the Dark Cosmology Centre funded by The Danish National Research Foundation. J.S. acknowledges support from Danmarks Nationalbank, from the Anna-Greta and Holger Crafoord fund and from Knut & Alice Wallenberg foundation. CrAO and IKI acknowledge support from Russian Ministry of Education and Science. J.P.H. and N.M. acknowledge support from the National Science Foundation under grant 0206051. The research activities of J.G. and M.J. are supported by the Spanish Ministry of Science through projects AYA2004-01515 and ESP2005-07714-C03-03. Based in part on observations made with the BOOTES instruments in South Spain (ESAt-INTA/CEDEA, Huelva) and with the 1.5 m Telescope of Observatorio de Sierra Nevada (OSN), operated by IAA/CSIC. Some of the data presented here have been taken using ALFOSC, which is owned by the Instituto de Astrofísica de Andalucía (IAA) and operated at the Nordic Optical Telescope under agreement between IAA and the Depertment of Astronomy of Copenhagen University. Thanks to Tamara Davis for very careful reading of the manuscript, and for detailed discussions on K-corrections. Last but not least, we acknowledge support from several key observers that contributed to this work, namely V. Birykov and D. Sharapov as well as D. R. Rafferty & J. R. Thorstensen. Finally the late Hugo E. Schwarz contributed with observations and comments on an earlier version of this paper.

References

Allen, C. W. 2000, Allen's Astrophysical Quantities, 4th edition 2000, ed. A. N. Cox
Amati, L., Frontera, F., Tavani, M., et al. 2002, A&A, 390, 81
Amati, L., Della Valle, M., Frontera, F., et al. 2007, A&A, 463, 913
Assafin, M., Andrei, A. H., Martins, R., et al. 2001, ApJ, 552, 380
Band, D., Matteson, J., Ford, L., et al. 1993, ApJ, 413, 281
Barraud, C., Olive, J.-F., Lestrade, J. P., et al. 2003, A&A, 400, 1021
Barraud, C., Daigne, F., Mochkovitch, R., & Atteia, J. L. 2005, A&A, 440, 809
Bersier, D., Fruchter, A. S., Strogler, L.-G., et al. 2006, ApJ, 643, 284
Björnsson, G., Gudmundsson, E. H., & Johannesson, E. H. 2004, ApJ, 615, L77
Butler, N. R., Sakamoto, T., Suzuki, M., et al. 2005, ApJ, 621, 884
Campana, S., Barthelmy, S., Burrows, D., et al. 2005a, GCN, 3866
Campana, S., Mangano, V., Chincarini, G., et al. 2005b, GCN, 3872
Campana, S., Mangano, V., Blustin, A. J., et al. 2006, Nature, 442, 1008
Castro-Tirado, A. J., Jelinek, M., Mateo Sanguino, T. J., et al. 2004, Astron. Nachr., 325, 679
Cenko, S. B., Kulkarni, S. R., Gal-Yam, A., & Berger, E. 2005, GCN, 3542
Christensen, L., Hjorth, J., & Gorosabel, J. 2004, A&A, 425, 913
Crew, G., Ricker, G., Atteia, J.-L., et al. 2005, GCN, 3890
Dermer, C. D., Chiang, J., & Böttcher, M. 1999, ApJ, 513, 656
Deutsch, E. W. 1999, AJ, 118, 1882
Dickey, J. M., & Lockman, F. J. 1990, ARA&A, 28, 215
Fan, Y. Z., & Wei, D. M. 2005, MNRAS, 364, L42
Fukugita, M., Shimasaku, K., & Ichikawa, T. 1995, PASP, 107, 945
Fynbo, J., Sollerman, J., Hjorth, J., et al. 2004, ApJ, 609, 962
Fynbo, J. P. U., Jensen, B. L., Sollerman, J., et al. 2005, GCN, 3874
Fynbo, J. P. U., Watson, D., Thoene, C., et al. 2006, Nature, 444, 1047
Ghisellini, G., Ghirlanda, G., Mereghetti, S., et al. 2006, MNRAS, 372, 1699
Gorosabel, J., Christensen, L., Hjorth, J., et al. 2003, A&A, 400, 127
Gorosabel, J., Casanova, V., Garrido, R., et al. 2005, GCN, 3865
Gorosabel, J., Castro-Tirado, A. J., Ramirez-Ruiz, E., et al. 2006, ApJ, 641, L13
Granot, J., Ramirez-Ruiz, E., & Perna, R. 2005, ApJ, 630, 1003
Heise, J., in't Zand, J., Kippen, R. M., & Woods, P. M. 2001, in the Proc. of the conference, Gamma-ray Bursts in the Afterglow Era, 16
Hjorth, J., Sollerman, J., Møller, P., et al. 2003, Nature, 423, 847
Hjorth, J., et al. 2007, in prep.
Huang, Y. F., Gou, L. J., Dai, Z. G., & Lu, T. 2000, ApJ, 543, 90
Jakobsson, P., Hjorth, J., & Fynbo, J. P. U. 2004, A&A, 425, 785
Kennicutt, R. C. 1998, ARA&A, 36, 189
Kewley, L. J., & Dopita, M. A. 2002, ApJS, 142, 35
Kippen, R. M., Woods, P. M., Heise, J., et al. 2003, Gamma-Ray Burst and Afterglow Astronomy 2001: A Workshop Celebrating the First Year of the HETE Mission, AIP Conf. Proc., 662, 244
Krimm, H., Barbier, L., Barthelmy, S., et al. 2005, GCN, 3871
Kumar, P., & Piran, T. 2000, ApJ, 535, 152
Lamb, D. Q., Donaghy, T. Q., & Graziani, C. 2005, ApJ, 620, 355L
Landolt, A. U. 1992, AJ, 104, 340
Le Floch, E., Duc, P.-A., Mirabel, I. F., et al. 2003, A&A, 400, 499
Levan, A., Patel, S., Kouveliotou, C., et al. 2005, ApJ, 622, 977
Matheson, T., Garnavich, P. M., Stanek, K. Z., et al. 2003, ApJ, 599, 394
Mirabal, N., & Halpern, J. P. 2006, GCN, 4792
Mirabal, N., Halpern, J. P., An, D., et al. 2006, ApJ, 643, 99
Modjaz, M., Stanek, K. Z., Garnavich, P. M., et al. 2006, ApJ, 645, 21
Oke, J. B. 1990, AJ, 99, 1621
Pagel, B. E. J., Edmunds, M. G., Blackwell, D. E., Chun, M. S., & Smith, G. 1979, MNRAS, 189, 95
Pei, Y. C. 1992, ApJ, 395, 130
Pian, E., Mazzali, P., Masetti, N., et al. 2006, Nature, 442, 1011
Preece, R. D., Mallozzi, R. S., Pendleton, G. N., & Paciesas, W. S. 2000, ApJS, 126, 19
Rau, A., Salvato, M., & Greiner, J. 2005, A&A, 444, 425
Rhoads, J. E. 2003, ApJ, 591, 1097
Sakamoto, T., Lamb, D. Q., Kawai, N., et al. 2005, ApJ, 629, 311
Schady, P., Mason, K. O., Osborne, J. P., et al. 2006, ApJ, 643, 276
Schaefer, B. E., Yuang, F., & Alatalo, K. 2005, GCN, 3867
Schlegel, D. J., Finkbeiner, D. P., & Davis, M. 1998, ApJ, 500, 525
Soderberg, A. M., Kulkarni, S. R., Fox, D. B., et al. 2005, ApJ, 627, 877
Soderberg, A. M., Nakar, E., Cenko, S. B., et al. 2006 [arXiv:astro-ph/0607511]
Sollerman, J., Kozma, C., Fransson, C., et al. 2000, ApJ, 537, L127
Sollerman, J., Östlin, G., Fynbo, J. P. U., et al. 2005, New Astron., 11, 103
Sollerman, J., Jaunsen, A. O., Fynbo, J. P. U., et al. 2006, A&A, 454, 503
Tominaga, N., Deng, J., Mazzali, P. A., et al. 2004, ApJ, 612, L105
Turnshek, D. A., Rao, S. M., Ptak, A. F., Griffiths, R. E., & Monier, E. M. 2003, ApJ, 590, 730
Watson, D., Fynbo, J. P. U., Ledoux, C., et al. 2006, ApJ, 652, 1011
Wiersema, K., Savaglio, S., Vreeswijk, P. M., et al. 2007, A&A, 464, 529
Woosley, S. E., & Bloom, J. 2006, ARA&A, 44, 507
Woosley, S. E., Eastman, R. G., & Schmidt, B. P. 1999, ApJ, 516, 788
Yamazaki, R., Ioka, K., & Nakamura, T. 2002, ApJ, 571, L31
Yamazaki, R., Ioka, K., & Nakamura, T. 2003, ApJ, 593, 941
Zeh, A., Klose, S., & Hartmann, D. H. 2004, ApJ, 609, 952
Zhang, B., Fan, Y. Z., Dyks, J., et al. 2006, ApJ, 642, 354

Online Material

Table 2. Log of observations and photometry of the afterglow of XRF 050824.

Date (UT)	Δt (days)	Magnitude	Magnitude Error (1σ)	Passband	Telescope
Aug. 25.0973	0.130449	20.72	0.04	*B*-band	NOT
Aug. 25.1017	0.134850	20.72	0.05	*B*-band	NOT
Aug. 25.1061	0.139250	20.65	0.04	*B*-band	NOT
Oct. 6.1943	42.2274	24.43	0.16	*B*-band	VLT
Oct. 6.1898	42.2229	24.26	0.17	*V*-band	VLT
Aug. 24.9742	0.007346	18.22	0.35	*R*-band	BOOTES
Aug. 24.9813	0.014429	19.11	0.32	*R*-band	BOOTES
Aug. 24.9935	0.0266991	18.94	0.03	*R*-band	OSN
Aug. 24.9971	0.0302391	19.04	0.04	*R*-band	OSN
Aug. 25.0007	0.0338001	19.07	0.03	*R*-band	OSN
Aug. 25.0096	0.042705	19.67	0.33	*R*-band	BOOTES
Aug. 25.0166	0.0496998	19.31	0.03	*R*-band	OSN
Aug. 25.0337	0.0668297	19.56	0.05	*R*-band	OSN
Aug. 25.0372	0.0703697	19.59	0.07	*R*-band	OSN
Aug. 25.0546	0.0877495	19.80	0.04	*R*-band	NOT
Aug. 25.0609	0.0940495	19.85	0.05	*R*-band	NOT
Aug. 25.0653	0.0984497	19.93	0.04	*R*-band	NOT
Aug. 25.0881	0.121212	19.33	0.20	*R*-band	BOOTES
Aug. 25.1496	0.182749	20.15	0.04	*R*-band	OSN
Aug. 25.1599	0.193050	20.21	0.05	*R*-band	OSN
Aug. 25.1700	0.203150	20.23	0.07	*R*-band	OSN
Aug. 25.1813	0.214449	20.38	0.08	*R*-band	OSN
Aug. 25.2003	0.233429	20.42	0.10	*R*-band	MDM
Aug. 25.2042	0.237391	20.22	0.08	*R*-band	MDM
Aug. 25.2082	0.241360	20.42	0.10	*R*-band	MDM
Aug. 25.2122	0.245300	20.34	0.09	*R*-band	MDM
Aug. 25.2161	0.249279	20.39	0.09	*R*-band	MDM
Aug. 25.2201	0.253250	20.47	0.11	*R*-band	MDM
Aug. 25.2241	0.257210	20.51	0.12	*R*-band	MDM
Aug. 25.2251	0.258249	20.25	0.05	*R*-band	D1.5 m
Aug. 25.2280	0.261179	20.39	0.11	*R*-band	MDM
Aug. 25.2303	0.263451	20.47	0.06	*R*-band	D1.5 m
Aug. 25.2320	0.265150	20.35	0.11	*R*-band	MDM
Aug. 25.2360	0.269110	20.24	0.10	*R*-band	MDM
Aug. 25.2402	0.273399	20.35	0.07	*R*-band	MDM
Aug. 25.2477	0.280849	20.30	0.07	*R*-band	MDM
Aug. 25.2551	0.288280	20.49	0.08	*R*-band	MDM
Aug. 25.2626	0.295719	20.35	0.08	*R*-band	MDM
Aug. 25.2700	0.303150	20.39	0.07	*R*-band	MDM
Aug. 25.2783	0.311409	20.62	0.11	*R*-band	MDM
Aug. 25.2966	0.329741	20.43	0.05	*R*-band	MDM
Aug. 25.3040	0.337179	20.55	0.08	*R*-band	MDM
Aug. 25.3062	0.339350	20.64	0.09	*R*-band	D1.5 m
Aug. 25.3111	0.344250	20.69	0.10	*R*-band	D1.5 m
Aug. 25.3115	0.344610	20.51	0.08	*R*-band	MDM
Aug. 25.3288	0.361910	20.49	0.06	*R*-band	MDM
Aug. 25.3362	0.369339	20.62	0.07	*R*-band	MDM
Aug. 25.3436	0.376780	20.55	0.06	*R*-band	MDM
Aug. 25.3511	0.384220	20.60	0.07	*R*-band	MDM
Aug. 25.3587	0.391870	20.58	0.06	*R*-band	MDM
Aug. 25.3632	0.396349	20.55	0.05	*R*-band	VLT
Aug. 25.3661	0.399300	20.60	0.06	*R*-band	MDM
Aug. 25.3736	0.406740	20.60	0.06	*R*-band	MDM
Aug. 25.3810	0.414169	20.73	0.07	*R*-band	MDM
Aug. 25.3885	0.421610	20.59	0.06	*R*-band	MDM
Aug. 25.3959	0.429060	20.65	0.06	*R*-band	MDM
Aug. 25.4034	0.436510	20.71	0.07	*R*-band	MDM
Aug. 25.4108	0.443939	20.74	0.08	*R*-band	MDM
Aug. 25.4221	0.455200	20.57	0.08	*R*-band	MDM
Aug. 25.4295	0.462690	20.69	0.09	*R*-band	MDM
Aug. 25.4370	0.470129	20.66	0.09	*R*-band	MDM
Aug. 25.4444	0.477560	20.78	0.10	*R*-band	MDM
Aug. 25.4519	0.485001	20.83	0.11	*R*-band	MDM
Aug. 25.4593	0.492430	20.71	0.09	*R*-band	MDM
Aug. 25.4668	0.499910	20.73	0.11	*R*-band	MDM

Table 2. continued.

Date (UT)	Δt (days)	Magnitude	Magnitude Error (1σ)	Passband	Telescope
Aug. 25.4742	0.507349	20.82	0.11	*R*-band	MDM
Aug. 25.4816	0.514780	20.98	0.12	*R*-band	MDM
Aug. 25.4905	0.523621	20.71	0.10	*R*-band	MDM
Aug. 25.9037	0.936850	21.17	0.09	*R*-band	Maidanak
Aug. 26.0098	1.04295	21.34	0.10	*R*-band	NOT
Aug. 26.0148	1.04795	21.30	0.06	*R*-band	NOT
Aug. 26.2076	1.24075	21.42	0.09	*R*-band	VLT
Aug. 26.2083	1.24145	21.45	0.12	*R*-band	VLT
Aug. 26.2238	1.25695	21.57	0.11	*R*-band	D1.5 m
Aug. 26.2291	1.26225	21.47	0.10	*R*-band	D1.5 m
Aug. 26.2349	1.26805	21.35	0.10	*R*-band	D1.5 m
Aug. 26.2532	1.28635	21.47	0.07	*R*-band	VLT
Aug. 26.2921	1.32527	21.56	0.04	*R*-band	MDM
Aug. 26.3224	1.35553	21.67	0.05	*R*-band	MDM
Aug. 26.3525	1.38562	21.68	0.05	*R*-band	MDM
Aug. 26.3561	1.38925	21.63	0.15	*R*-band	D1.5 m
Aug. 26.3609	1.39405	21.59	0.11	*R*-band	D1.5 m
Aug. 26.3748	1.40791	21.71	0.06	*R*-band	MDM
Aug. 27.3055	2.33870	21.90	0.05	*R*-band	MDM
Aug. 27.3438	2.37690	21.77	0.05	*R*-band	MDM
Aug. 28.0352	3.06835	22.17	0.08	*R*-band	NOT
Aug. 28.0508	3.08395	22.09	0.06	*R*-band	NOT
Aug. 28.3367	3.36986	22.08	0.04	*R*-band	MDM
Aug. 29.3194	4.35259	22.18	0.05	*R*-band	MDM
Aug. 30.1455	5.17865	22.22	0.06	*R*-band	WHT
Sep. 2.2300	8.26315	22.64	0.13	*R*-band	D1.5 m
Sep. 3.8139	9.84705	22.68	0.12	*R*-band	CrAO2.6
Sep. 4.8392	10.8724	23.00	0.08	*R*-band	CrAO2.6
Sep. 11.1326	17.1657	22.76	0.07	*R*-band	NOT
Sep. 14.4278	20.4609	22.95	0.06	*R*-band	MDM
Sep. 16.8254	21.8582	22.70	0.60	*R*-band	Maidanak
Sep. 29.3190	35.3521	23.59	0.09	*R*-band	MDM
Sep. 29.8556	35.8887	23.44	0.13	*R*-band	NOT
Oct. 6.1914	42.2245	23.72	0.09	*R*-band	VLT
Oct. 7.8490	43.8821	24.00	0.30	*R*-band	CrAO2.6
Nov. 7.7356	74.7687	23.94	0.23	*R*-band	CrAO2.6
Dec. 7.0694	104.1025	23.70	0.15	*R*-band	NTT
Aug. 25.0032	0.0363503	18.84	0.06	*I*-band	OSN
Aug. 25.0067	0.0398502	18.84	0.05	*I*-band	OSN
Aug. 25.0254	0.0585499	19.26	0.06	*I*-band	OSN
Aug. 25.0391	0.0722	19.11	0.06	*I*-band	OSN
Aug. 25.0426	0.0757504	19.38	0.07	*I*-band	OSN
Aug. 25.0753	0.108450	19.48	0.05	*I*-band	NOT
Aug. 25.0796	0.112749	19.57	0.07	*I*-band	NOT
Aug. 25.0870	0.120150	19.50	0.04	*I*-band	NOT
Aug. 25.1521	0.185249	19.84	0.08	*I*-band	OSN
Aug. 25.1730	0.206150	19.92	0.08	*I*-band	OSN
Aug. 25.1838	0.216949	19.98	0.09	*I*-band	OSN
Aug. 25.2602	0.293350	19.97	0.09	*I*-band	D1.5 m
Aug. 25.2661	0.299250	19.93	0.08	*I*-band	D1.5 m
Aug. 25.3527	0.385849	20.10	0.07	*I*-band	D1.5 m
Aug. 25.3659	0.399050	20.12	0.08	*I*-band	D1.5 m
Aug. 26.3472	1.3804	19.03	0.05	K-band	VLT